Magn. Reson., 5, 121–129, 2024
https://doi.org/10.5194/mr-5-121-2024

Open Access
MAGNETIC RESONANCE

^{1}H-enhanced ^{103}Rh NMR spectroscopy and relaxometry of ^{103}Rh(acac)$_3$ in solution

Harry Harbor-Collins[1], **Mohamed Sabba**[1], **Markus Leutzsch**[2], **and Malcolm H. Levitt**[1]

[1]School of Chemistry, University of Southampton, SO17 1BJ, Southampton, UK
[2]Service Department NMR Spectroscopy, Max-Planck-Institut für Kohlenforschung, Kaiser-Wilhelm-Platz 1, 45470 Mülheim an der Ruhr, Germany

Correspondence: Malcolm H. Levitt (mhl@soton.ac.uk)

Received: 30 May 2024 – Discussion started: 5 June 2024
Revised: 5 July 2024 – Accepted: 9 July 2024 – Published: 30 August 2024

Abstract. Recently developed polarisation transfer techniques are applied to the ^{103}Rh nuclear magnetic resonance (NMR) of the ^{103}Rh(acac)$_3$ coordination complex in solution. Four-bond ^{1}H–^{103}Rh J couplings of around 0.39 Hz are exploited to enhance the ^{103}Rh NMR signal and to estimate the ^{103}Rh T_1 and T_2 relaxation times as a function of field and temperature. The ^{103}Rh longitudinal T_1 relaxation in ^{103}Rh(acac)$_3$ is shown to be dominated by the spin–rotation mechanism, with an additional field-dependent contribution from the ^{103}Rh chemical shift anisotropy.

1 Introduction

Although rhodium is one of the few chemical elements with a 100 % abundant spin-1/2 isotope, the routine nuclear magnetic resonance (NMR) of ^{103}Rh has been inhibited by its very small gyromagnetic ratio, which is negative and $\sim$ 31.59 times less than that of ^{1}H (Mann, 1991).

While indirectly detected ^{103}Rh NMR has had an appreciable history (Crocker et al., 1979; Dykstra et al., 1981; Brevard and Schimpf, 1982; Heaton et al., 1983; Brevard et al., 1981; Herberhold et al., 1999; Ernsting et al., 2004; Carlton, 2008), advances in instrumentation and methodology have allowed rapid observation of ^{103}Rh NMR parameters on standard commercial NMR spectrometers, leading to a recent renaissance of the field (Chan et al., 2020; Bajo et al., 2020; Wiedemair et al., 2021; Widemann et al., 2021; Rösler et al., 2021; Sheng Loong Tan et al., 2021; Caló et al., 2021; Samultsev et al., 2022; Harbor-Collins et al., 2023, 2024; Holmes et al., 2023; Lutz et al., 2023).

The rhodium (III) acetylacetonate (^{103}Rh(acac)$_3$) complex (see Fig. 1) currently serves as the International Union of Pure and Applied Chemistry (IUPAC) ^{103}Rh NMR chemical-shift reference (Carlton, 2008). To the wider scientific community, ^{103}Rh(acac)$_3$ is better known for its role in the production of thin rhodium films and nanocrystals for use in catalysis (Zhang et al., 2007; Aaltonen et al., 2005; Choi et al., 2016).

The early studies of nuclear spin relaxation in ^{103}Rh(acac)$_3$ were greatly limited by the poor ^{103}Rh signal strength, and they provided somewhat conflicting conclusions for the ^{103}Rh relaxation mechanisms (Grüninger et al., 1980; Benn et al., 1985; Maurer et al., 1982). Recently, a two-bond ^{13}C–^{103}Rh coupling of 1.1 Hz was observed in ^{103}Rh(acac)$_3$ and was exploited for triple-resonance experiments (Caló et al., 2021).

We now report the observation of a four-bond ^{1}H–^{103}Rh J coupling of $|^{4}J_{\mathrm{HRh}}| \simeq 0.39$ Hz between the central ^{103}Rh nucleus and each of the three methine ^{1}H nuclei in ^{103}Rh(acac)$_3$ (see Fig. 1). These small couplings are exploited for the ^{1}H-enhanced ^{103}Rh NMR spectroscopy of the ^{103}Rh(acac)$_3$ complex. ^{103}Rh spin–lattice T_1 and spin–spin T_2 relaxation time constants are measured over a range of magnetic fields and temperatures. The ^{103}Rh T_1 relaxation is found to be dominated by spin–rotation, with an additional contribution from the chemical shift anisotropy (CSA), which is significant at high fields.

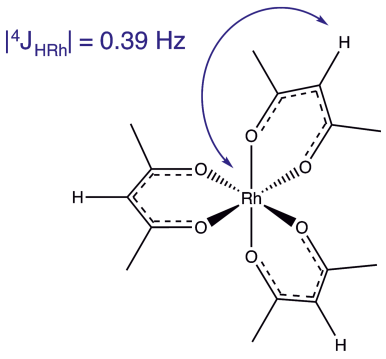

Figure 1. The molecular structure of rhodium (III) acetylacetonate, ^{103}Rh(acac)$_3$, which has point group symmetry D_3. This work exploits the long-range $^{4}J_{\mathrm{HRh}}$ scalar couplings for polarisation transfer between the ^{103}Rh and methine ^{1}H spins.

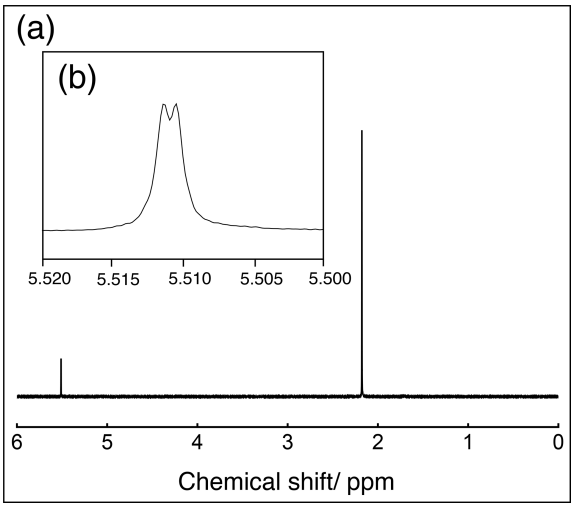

Figure 2. (a) ^{1}H spectrum of a $\sim$ 140 mM solution of ^{103}Rh(acac)$_3$ in $CDCl_3$, acquired at 9.4 T and 298 K, in a single transient. Lorentzian line broadening (1 Hz) was applied. **(b)** Expanded view of the methine ^{1}H resonance. Negative Lorentzian line broadening (−0.2 Hz) was applied to enhance the resolution.

2 Experimental

Experiments were performed on a saturated ($\sim$ 140 mM) solution of rhodium (III) acetylacetonate (^{103}Rh(acac)$_3$) dissolved in 350 µL $CDCl_3$. ^{103}Rh(acac)$_3$ was purchased from Sigma-Aldrich and used as received. ^{103}Rh(acac)$_3$ is a bright yellow powder, which is dissolved in $CDCl_3$ to form a solution with a deep golden colour.

The radio frequency channels were additionally isolated by installing a bandpass (K&L Microwave) and low-pass (Chemagnetics 30 MHz) filter at the preamplifier outputs of the ^{1}H and ^{103}Rh channels, respectively. Pulse powers on the ^{1}H and ^{103}Rh channels were calibrated to give a matched nutation frequency of $2\pi \times 4000$ Hz, corresponding to a 90° pulse length of 62.5 µs. Field-cycling experiments were performed using a motorised fast-shuttling system (Zhukov et al., 2018; Harbor-Collins et al., 2023, 2024). The shuttling time was kept constant at 2 s, in both directions.

3 Results

3.1 ^{1}H spectrum

The ^{1}H spectrum for ^{103}Rh(acac)$_3$ in $CDCl_3$ (shown in Fig. 2a) features two resonances: a singlet at 2.170 ppm, corresponding to the six methyl protons on each acac ligand, and a broad, weak doublet centred at 5.511 ppm, corresponding to the acac methine protons. An expanded region showing just the methine resonance is presented in Fig. 2b. The four-bond ^{103}Rh–^{1}H spin–spin coupling is estimated to be $|^{4}J_{\mathrm{HRh}}| = 0.39 \pm 0.01$ Hz.

3.2 ^{103}Rh spectra

3.2.1 Direct ^{103}Rh excitation

The ^{1}H-decoupled ^{103}Rh spectrum of the ^{103}Rh(acac)$_3$ solution, acquired with single-pulse excitation of ^{103}Rh transverse magnetisation, is shown in Fig. 3a and displays a single peak with the ^{103}Rh chemical shift of 8337.6 ppm. The signal-to-noise ratio is quite poor, even after 12 h of data acquisition.

3.2.2 ^{1}H–^{103}Rh polarisation transfer by DualPol

Polarization transfer from the ^{1}H nuclei to the ^{103}Rh nuclei was performed using the previously described DualPol pulse sequence incorporating acoustic-ringing suppression (Harbor-Collins et al., 2023), as shown in Fig. 4.

The DualPol sequence consists of two synchronised PulsePol sequences (Schwartz et al., 2018), applied simultaneously on two radio frequency channels.

The PulsePol sequence was originally developed in the context of electron–nucleus polarisation transfer (Schwartz et al., 2018). As discussed in Sabba et al. (2022), PulsePol may be interpreted as a "riffled" implementation of an R sequence, using the nomenclature of symmetry-based recoupling in solid-state NMR (Carravetta et al., 2000). In the case of PulsePol, the R element is a composite $90_y 180_x 90_y$ pulse, with "windows" inserted between the pulses. Furthermore, in the current implementation, the central 180_x pulse of each R element is itself substituted by a BB1 composite pulse (Wimperis, 1994). That substitution was previously shown to increase the robustness of the pulse sequence with respect to deviations in the radio frequency amplitudes and resonance offsets (Sabba et al., 2022). The total R-element duration, including all pulses and windows, is denoted using τ_{R} here (see Fig. 4).

For the experiments described here, the DualPol sequences used an R-element duration equal to $\tau_{\mathrm{R}} = 70$ ms, with pulse

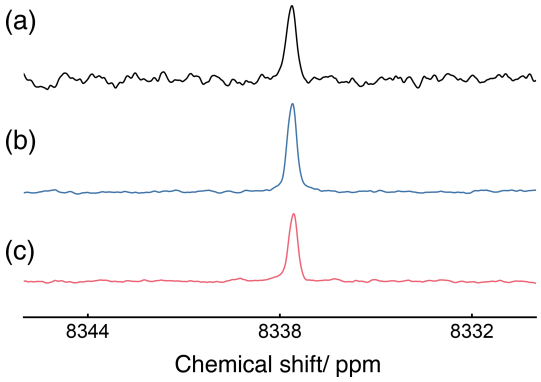

Figure 3. ^{1}H-decoupled ^{103}Rh NMR spectra of a $\sim$140 mM solution of ^{103}Rh(acac)$_3$ in $CDCl_3$, in a field of 9.4 T and at a temperature of 295 K. Lorentzian line broadening (1 Hz) was applied to all spectra. ^{103}Rh chemical shifts are referenced to the absolute frequency ($\Xi(^{103}\text{Rh}) = 3.16\,\%$). In all spectra, ^{1}H decoupling was achieved using continuous wave decoupling with 0.05 W of power, corresponding to a nutation frequency of 1 kHz. **(a)** ^{103}RhHdec spectrum, acquired using 300 transients, each using a single ^{103}Rh 90° pulse. The waiting interval between transients was 150 s. The total experimental duration was $\sim$12 h. **(b)** ^{103}RhHdec spectrum, acquired using 16 transients and the pulse sequence shown in Fig. 4, with $n = 11$ repetitions of the DualPol (dual-channel PulsePol) sequence. The waiting interval between transients was 18 s. The total experimental duration was 5 min. **(c)** ^{103}RhHdec spectrum, acquired using 16 transients and an optimised refocused-INEPT (Insensitive Nucleus Enhancement by Polarisation Transfer) sequence. The waiting interval between transients was 18 s. The total experimental duration was 5 min.

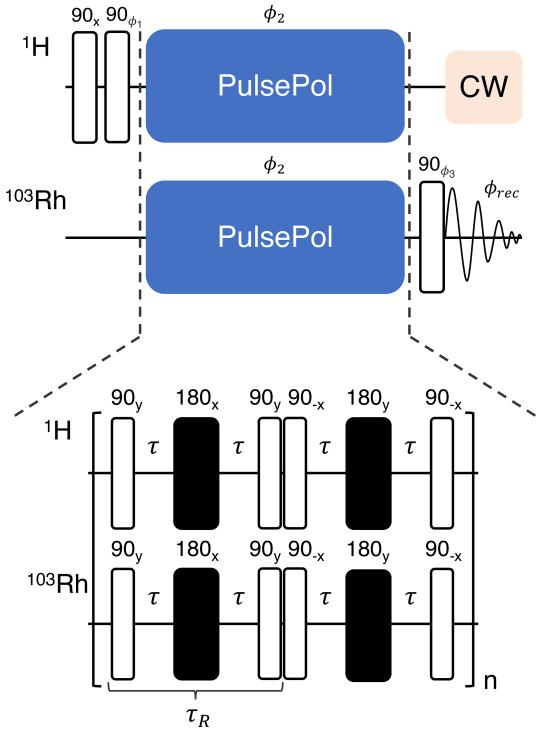

Figure 4. Pulse sequence for the acquisition of ^{1}H-enhanced ^{103}Rh spectra; an expanded view of the DualPol pulse sequence module is shown at the bottom. The black rectangles indicate symmetrised BB1 composite 180° pulses (Wimperis, 1994; Cummins et al., 2003) and τ indicates an interpulse delay. Phase cycles are given by the following: $\phi_1 = [-x, x, -x, x]$, $\phi_2 = [x, x, -x, -x]$, $\phi_3 = [x, x, x, x, y, y, y, y, -x, -x, -x, -x, -y, -y, -y, -y]$ and the receiver $\phi_{\text{rec}} = [x, -x, x, -x, y, -y, y, -y, -x, x, -x, x, -y, y, -y, y]$.

durations given by $\tau_{90} = 62.5\,\mu$s for the 90° pulses and $\tau_{\text{BB1}} = 10 \times \tau_{90} = 625\,\mu$s for the BB1 composite 180° pulses.

The ^{103}Rh and methine ^{1}H nuclei of ^{103}Rh(acac)$_3$ form an I_3S spin system, where the ^{103}Rh nucleus is the S spin and the magnetically equivalent ^{1}H nuclei are the I spins.

The DualPol spin dynamics are identical to those for Hartmann–Hahn J cross-polarisation (Chingas et al., 1981). The DualPol average Hamiltonian has the following form:

$$\overline{H}^{(1)} = \kappa \times 2\pi J_{\text{IS}}(\text{I}_x S_x + \text{I}_y S_y), \tag{1}$$

where the scaling factor is given by $\kappa = 1/2$ in the limit of short, ideal, radio frequency pulses. In the absence of relaxation and pulse imperfections, a DualPol sequence with a scaling factor $\kappa = 1/2$, applied to an I_3S spin system should give rise to the following enhancement of the S-spin magnetisation, relative to its thermal-equilibrium value:

$$\epsilon_{\text{DualPol}}(T) = \frac{\gamma_{\text{I}}}{4\gamma_{\text{S}}}\left\{2\sin^2\left(\frac{1}{2}J_{\text{IS}}T\right) + \sin^2(\pi J_{\text{IS}}T) + 2\sin^2\left(\frac{1}{2}\sqrt{3}\pi J_{\text{IS}}T\right)\right\}. \tag{2}$$

Here, T is the overall duration of the DualPol sequence. As the magnetogyric ratios of ^{103}Rh and ^{1}H have opposite signs, the function $\epsilon_{\text{DualPol}}(T)$ is negative for all values of T. The blue curve in Fig. 5 shows a plot of $|\epsilon_{\text{DualPol}}|$ against T, for a J coupling of $|J_{\text{IS}}| \simeq 0.39$ Hz. The maximum value of $|\epsilon_{\text{DualPol}}|$ is given in the absence of relaxation by

$$\left|\epsilon^{\text{max}}_{\text{DualPol}}\right| = |17\gamma_{\text{I}}/16\gamma_{\text{S}}| \simeq 33.56 \tag{3}$$

for the case of I = ^{1}H and S = ^{103}Rh. As Eq. (2) is quasi-periodic (Chingas et al., 1981), the value of T which maximises $|\epsilon_{\text{DualPol}}|$ is indeterminate. The first maximum may be found numerically and occurs at the duration $T_{1\text{st max}} \simeq 0.6098 J_{\text{IS}}^{-1}$, at which point the theoretical enhancement is given by $|\epsilon_{\text{DualPol}}| \simeq 1.052|\gamma_{\text{I}}/\gamma_{\text{S}}| \simeq 33.23$ for the case of I = ^{1}H and S = ^{103}Rh. Hence, for the estimated ^{1}H–^{103}Rh J coupling of $|J_{\text{IS}}| \simeq 0.39$ Hz, assuming $\kappa = 1/2$, the ^{103}Rh signal enhancement is expected to reach its first maximum at a DualPol duration of $T_{1\text{st max}} \simeq 1.563$ s, in the absence of relaxation.

In the experiments described here, the optimum duration of the DualPol sequence was found for a repetition number of $n = 11$. For an R-element duration of $\tau_{\text{R}} = 70$ ms, this cor-

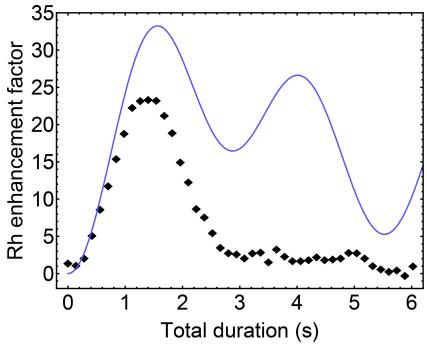

Figure 5. ^{103}Rh signal enhancement factor for ^{103}Rh(acac)$_3$ as a function of DualPol sequence duration T, normalised against thermal-equilibrium ^{103}Rh polarisation. Black diamonds: experimental data points; solid blue line: the theoretical enhancement factor $|\epsilon_{\mathrm{DualPol}}(T)|$ for an $\mathrm{I_3\,S}$ spin system in the absence of relaxation, as given by Eq. (2) for $|J_{\mathrm{IS}}| = 0.39$ Hz.

responds to a total DualPol sequence duration of $T = 1.54$ s, which is in good agreement with the theoretical value.

The DualPol-enhanced ^{103}Rh spectrum is shown in Fig. 3b and displays an experimental signal enhancement of ~ 23 over the directly excited ^{103}Rh spectrum in Fig. 3a.

Figure 5 shows the experimental ^{103}Rh signal enhancement factor as a function of the DualPol sequence duration T. Although the maximum of the experimental enhancement occurs at a similar position to the maximum of the theoretical curve, there is clearly a strong damping of the enhancement with respect to the duration T, leading to a loss of intensity at the theoretical maximum. This damping may be associated with transverse relaxation of the ^{1}H and ^{103}Rh transverse magnetisation during the polarisation transfer process.

3.2.3 ^{1}H–^{103}Rh polarisation transfer by refocused INEPT

Polarisation transfer from ^{1}H to ^{103}Rh may also be conducted by the standard refocused-INEPT pulse sequence (Burum and Ernst, 1980). In this case, the theoretical enhancement of the S-spin magnetisation, due to transfer from the I spins, is given for the $\mathrm{I_3\,S}$ case, in the absence of relaxation and other imperfections, by Burum and Ernst (1980):

$$\epsilon_{\mathrm{RI}}(\tau_1, \tau_2) = \frac{3\gamma_{\mathrm{I}}}{4\gamma_{\mathrm{S}}} \sin(\pi J_{\mathrm{IS}} \tau_1) \times (\sin(\pi J_{\mathrm{IS}} \tau_2) + \sin(3\pi J_{\mathrm{IS}} \tau_2)), \quad (4)$$

where τ_1 and τ_2 refer to the total echo durations including two inter-pulse intervals, as shown in Fig. 1 of Burum and Ernst (1980). The maximum of this function is found at $\tau_1 = (2J_{\mathrm{IS}})^{-1}$ and $\tau_2 = \arcsin(3^{-1/2})/(\pi J_{\mathrm{IS}})$, giving an enhancement of $|\epsilon_{\mathrm{RI}}| = |2\gamma_{\mathrm{I}}/\sqrt{3}\gamma_{\mathrm{S}}|$ (Doddrell et al., 1981, 1982; Pegg et al., 1981, 1982). Therefore, the maximum theoretical enhancement by refocused INEPT is

$$\left|\epsilon_{\mathrm{RI}}^{\mathrm{max}}\right| = |2\gamma_{\mathrm{I}}/\sqrt{3}\gamma_{\mathrm{S}}| \simeq 1.155|\gamma_{\mathrm{I}}/\gamma_{\mathrm{S}}| \simeq 36.48 \quad (5)$$

for the case of $\mathrm{I} = {}^{1}$H and $\mathrm{S} = {}^{103}$Rh. Hence, in the absence of relaxation, refocused INEPT can give a slightly greater enhancement than DualPol in an $\mathrm{I_3\,S}$ system. However, the maximum enhancements by both DualPol and INEPT are less than the theoretical bound on the enhancement of S-spin magnetisation by polarisation transfer from the I spins in a permutation-symmetric $\mathrm{I_3\,S}$ spin system, which is equal to $|3\gamma_{\mathrm{I}}/2\gamma_{\mathrm{S}}|$ (Nielsen et al., 1995).

The theoretical advantage of INEPT over DualPol is not realised in practice for the case of ^{103}Rh(acac)$_3$. The maximum enhancement by refocused INEPT was realised for durations of $\tau_1 = 920$ and $\tau_2 = 500$ ms, which yielded a ^{103}Rh enhancement factor of ~ 17 over thermal polarisation, i.e. less than the maximum DualPol enhancement, which was ~ 23. The experimentally optimised interval τ_1 is significantly shorter than the optimum theoretical value in the absence of relaxation, which is $\tau_1^{\mathrm{theor}} = 1.28$ s, assuming a ^{103}Rh–^{1}H spin–spin coupling of $J_{\mathrm{HRh}} = 0.39$ Hz. The optimum value of τ_2, on the other hand, is very similar to the theoretical value, which is $\tau_2^{\mathrm{theor}} = 503$ ms.

The ^{1}H-enhanced ^{103}Rh spectrum, produced by an optimised refocused-INEPT sequence, is shown in Fig. 3c. It shows a significantly lower enhancement than the DualPol result of Fig. 3b, despite the fact that the theoretical enhancement by refocused INEPT is higher than that of DualPol in the absence of relaxation (see Eqs. 3 and 5). The loss of amplitude relative to the theoretical values may be attributed to transverse ^{1}H relaxation during the polarisation transfer process. It is known that Hartmann–Hahn-style cross-polarisation sequences such as DualPol can outperform INEPT in the presence of transverse relaxation (Levitt, 1991).

4 ^{1}H-detected ^{103}Rh T_2

The ^{103}Rh T_2 relaxation time constant for ^{103}Rh(acac)$_3$ in $CDCl_3$ was measured via the methine ^{1}H signals using a variant of a previously described indirectly detected T_2 DualPol pulse sequence (Harbor-Collins et al., 2023), which is shown in Fig. 6. The pulse sequence starts with a DualPol sequence of duration $T = 1.54$ s to transfer thermal-equilibrium longitudinal ^{1}H magnetisation to ^{103}Rh. The ^{103}Rh longitudinal magnetisation is converted into ^{103}Rh transverse magnetisation by a 90° pulse on the ^{103}Rh channel. The ^{103}Rh transverse magnetisation evolves under a Carr–Purcell–Meiboom–Gill (CPMG) train of m spin echoes, each with an echo duration $\tau_{\mathrm{echo}} = 45$ ms. The Carr–Purcell sequence suppresses the confounding effects of translational diffusion and mixing with antiphase spin operators (Peng et al., 1991). The ^{103}Rh transverse magnetisation is converted to ^{103}Rh longitudinal magnetisation by a second 90° ^{103}Rh pulse. A ^{1}H "D-filter" module is applied to destroy any residual ^{1}H magnetisation, before another DualPol

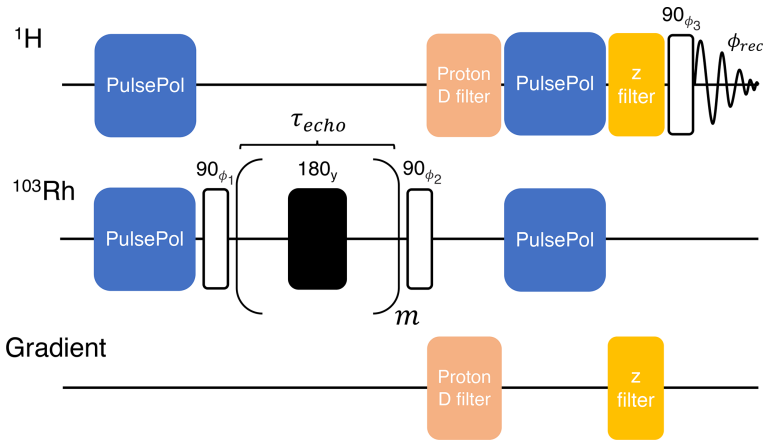

Figure 6. Sequence used for the indirect measurement of rhodium T_2 through ^{1}H detection. The phase cycles are given by the following: $\phi_1 = [x, x, -x, -x]$, $\phi_2 = [-x, x, -x, x]$, $\phi_3 = [x, x, x, x, y, y, y, y, -x, -x, -x, -x, -y, -y, -y, -y]$ and the receiver $\phi_{\text{rec}} = [x, -x, -x, x, y, -y, -y, y, -x, x, x, -x, -y, y, y, -y]$. The echo interval τ_{echo} was 45 ms. The black rectangle indicates a symmetrised BB1 composite 180° pulse (Wimperis, 1994; Cummins et al., 2003). An MLEV-64 supercycle was applied to the phases of the 180° pulses (Levitt et al., 1982a, b; Freeman et al., 1982; Gullion et al., 1990; Gullion, 1993). The ^{1}H "D-filter" and "z-filter" modules are described in Figs. 3 and 4 of Harbor-Collins et al. (2023), respectively.

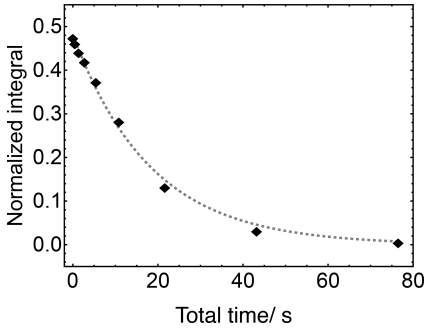

Figure 7. Decay curve for the ^{103}Rh transverse magnetisation of ^{103}Rh(acac)$_3$ in solution at a field of 9.4 T, measured by the indirectly detected multiple spin-echo scheme in Fig. 6. The experimental duration was 15 min.

sequence of duration $T = 1.54$ s transfers the ^{103}Rh longitudinal magnetisation to ^{1}H longitudinal magnetisation. A ^{1}H "z-filter" module is applied to destroy any other ^{1}H magnetisation components, followed by a 90° ^{1}H pulse which excites ^{1}H transverse magnetisation whose precession induces a ^{1}H NMR signal which is detected in the following interval. The ^{1}H D-filter and z-filter modules are described in Figs. 3 and 4 of Harbor-Collins et al. (2023), respectively.

Repetition of the experiment with increasing values of m leads to the ^{103}Rh T_2 decay curve shown in Fig. 7. This fits well to a single exponential decay with the time constant $T_2(^{103}\text{Rh}) = 18.36 \pm 0.92$ s.

5 ^{1}H-detected ^{103}Rh T_1

The ^{103}Rh T_1 relaxation time constant for ^{103}Rh(acac)$_3$ in $CDCl_3$ was measured indirectly using the methine ^{1}H signals, by means of the pulse sequence shown in Fig. 8 (Harbor-Collins et al., 2023). The pulse sequence starts with a DualPol sequence of duration $T = 1.54$ s to transfer thermal-equilibrium longitudinal ^{1}H magnetisation to ^{103}Rh. For variable-field experiments, the sample is shuttled out of the high-field magnet into a low-field region. The nuclear magnetisation is allowed to relax for an interval τ_{relax}. If necessary, the sample is shuttled back into high field, and residual ^{1}H magnetisation is destroyed by a ^{1}H D-filter module. A pair of phase-cycled 90° ^{103}Rh pulses are applied to select for ^{103}Rh z-magnetisation before a second DualPol sequence of duration $T = 1.54$ s transfers the partially relaxed longitudinal ^{103}Rh magnetisation to ^{1}H magnetisation. A ^{1}H z-filter module is applied to destroy any other ^{1}H magnetisation components, followed by a 90° ^{1}H pulse which excites ^{1}H transverse magnetisation whose precession induces a ^{1}H NMR signal that is detected in the following interval. The ^{1}H D-filter and z-filter modules are described in Figs. 3 and 4 of Harbor-Collins et al. (2023), respectively. During τ_{relax}, ^{1}H-enhanced ^{103}Rh magnetisation decays toward thermal ^{103}Rh magnetisation, which is very small; hence, at large values of τ_{relax}, resulting ^{103}Rh-derived ^{1}H signals are very weak and close to zero, even for measurements performed at higher magnetic field strengths.

The trajectory of indirectly detected ^{103}Rh z-magnetisation in a field of 9.4 T and at a temperature of 295 K is shown in Fig. 9a. The trajectory fits well to a single exponential decay with time constant $T_1(^{103}\text{Rh}) = 41.8 \pm 0.9$ s. A trajectory in the low magnetic field of 10 mT and at a

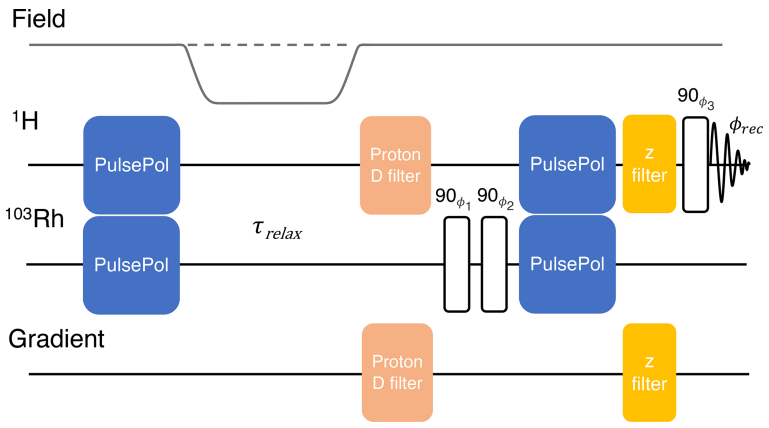

Figure 8. Sequence used for the indirect measurement of the rhodium T_1 through the ^{1}H NMR signal. Phase cycles are given by the following: $\phi_1 = [x, x, -x, -x]$, $\phi_2 = [-x, x, -x, x]$, $\phi_3 = [x, x, x, x, y, y, y, y, -x, -x, -x, -x, -y, -y, -y, -y]$ and the receiver $\phi_{rec} = [x, -x, -x, x, y, -y, -y, y, -x, x, x, -x, -y, y, y, -y]$. The optional shuttling of the sample to low field, and back again, during the interval τ_{relax} is indicated. The ^{1}H "D-filter" and "z-filter" modules are described in Figs. 3 and 4 of Harbor-Collins et al. (2023), respectively.

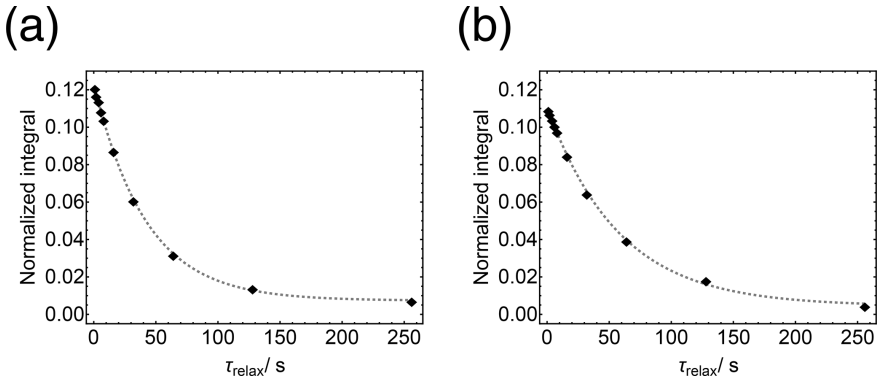

Figure 9. Trajectories of longitudinal ^{103}Rh magnetisation for ^{103}Rh(acac)$_3$ in solution at a temperature of 295 K, measured indirectly through the methine ^{1}H signals, using the pulse sequence in Fig. 8. **(a)** Filled symbols: ^{1}H signal amplitudes at a magnetic field of 9.4 T. The data were acquired in $\sim$2 h. The integrals are normalised against the ^{1}H spectrum obtained by a single ^{1}H 90° pulse applied to a system in thermal equilibrium at 9.4 T and at 295 K. Dotted line: fitted exponential decay with time constant $T_1(^{103}\text{Rh}) = 41.8 \pm 0.9$ s. Panel **(b)** is the same as panel **(a)** but the sample is shuttled to a field of 10 mT during the relaxation delay τ_{relax}. Dotted line: fitted exponential decay with time constant $T_1(^{103}\text{Rh}) = 57.8 \pm 1.7$ s.

temperature of 295 K is shown in Fig. 9b. This was produced by shuttling the sample to a low magnetic field, and back again, during the interval τ_{relax}. The relaxation process is somewhat slower in a low magnetic field, with a time constant of $T_1(^{103}\text{Rh}) = 57.8 \pm 1.7$ s.

The observed field dependence of the ^{103}Rh relaxation rate constant T_1^{-1} is shown in Fig. 10a. The magnetic field dependence of T_1^{-1} is quite weak in this range of fields. The relaxation rate constant increases slightly with increasing magnetic field at the high-field end, suggestive of a weak relaxation contribution from the ^{103}Rh chemical shift anisotropy. The blue curve in Fig. 10a shows the best-fit quadratic function $T_1^{-1}(B) = T_1^{-1}(0) + aB^2$, where $T_1^{-1}(0) = (167 \pm 7) \times 10^{-4}\,\text{s}^{-1}$ and $a = (7 \pm 2) \times 10^{-5}\,\text{s}^{-1}\,\text{T}^{-2}$.

The observed temperature dependence of the ^{103}Rh relaxation rate constant T_1^{-1} is shown for a field of $B \simeq 9.4$ T in Fig. 10b. The rhodium T_1^{-1} increases monotonically with increasing temperature over the relevant temperature range. At 315 K, relaxation occurs with a time constant of $T_1(^{103}\text{Rh}) = 30.6 \pm 1.1$ s.

A positive dependence of the ^{103}Rh T_1^{-1} on temperature was reported previously for ^{103}Rh(acac)$_3$ in solution (Benn et al., 1985).

6 Discussion

The temperature dependence of the ^{103}Rh T_1^{-1}, as shown in Fig. 10b, indicates a dominant spin–rotation relaxation mechanism. For small molecules with a short rotational correlation time relative to the nuclear Larmor period, spin–

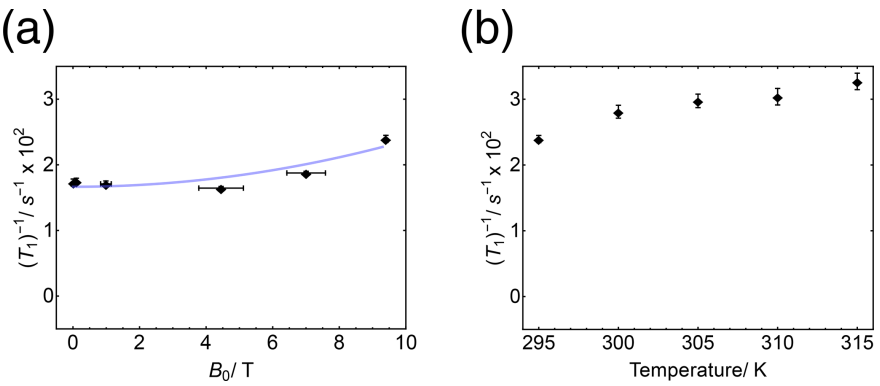

Figure 10. **(a)** ^{103}Rh relaxation rate constant T_1^{-1} for ^{103}Rh(acac)$_3$ in solution, as a function of magnetic field strength at a temperature of 295 K. The blue line shows the best-fit quadratic function $T_1^{-1}(B) = T_1^{-1}(0) + aB^2$, where $T_1^{-1}(0) = (167 \pm 7) \times 10^{-4}\,\mathrm{s}^{-1}$ and $a = (7 \pm 2) \times 10^{-5}\,\mathrm{s}^{-1}\,\mathrm{T}^{-2}$. **(b)** ^{103}Rh relaxation rate constant T_1^{-1} for ^{103}Rh(acac)$_3$ in solution, as a function of temperature at a magnetic field strength of 9.4 T.

rotation is the only mechanism that leads to a positive correlation of T_1^{-1} with temperature (Hubbard, 1963). This is because the amplitudes of the local magnetic fields generated by the spin–rotation interaction are proportional to the root-mean-square rotational angular momentum of the participating molecules – a quantity that is linked to the mean rotational kinetic energy of the molecules, which increases linearly with temperature. For other mechanisms, the decrease in the rotational correlation time τ_c with increasing temperature leads to a decrease in the relaxation rate with increasing temperature, in the fast-motion limit.

The field dependence of the ^{103}Rh T_1^{-1}, as shown in Fig. 10a, displays a modest increase in relaxation rate with increasing magnetic field at high field, which suggests an additional contribution from the rotational modulation of the ^{103}Rh CSA tensor. A finite ^{103}Rh CSA tensor is allowed with respect to symmetry under the D_3 point group of ^{103}Rh(acac)$_3$ (Buckingham and Malm, 1971). Indeed, solid-state NMR data indicate a ^{103}Rh shielding anisotropy of $\Delta\sigma \simeq 460$ ppm, with relativistic quantum chemistry calculations in reasonable agreement (Holmes et al., 2023). The magnitude of this CSA tensor is modest by ^{103}Rh standards. For example, the ^{103}Rh nuclei in Rh paddlewheel complexes have a shielding anisotropy of $|\Delta\sigma| \sim 9900$ ppm (Harbor-Collins et al., 2023).

In summary, we have demonstrated the successful transfer of polarisation between the central ^{103}Rh nucleus and the three methine ^{1}H nuclei in ^{103}Rh(acac)$_3$, through the very small four-bond ^{1}H–^{103}Rh couplings. The polarisation transfer is more efficient for DualPol than for refocused INEPT, even though the theoretical efficiency of DualPol is slightly less than that of refocused INEPT, for the relevant I_3S spin system. We have successfully exploited ^{1}H–^{103}Rh polarisation transfer to study the longitudinal and transverse relaxation of ^{103}Rh for ^{103}Rh(acac)$_3$ in solution. The ^{103}Rh T_1 relaxation is dominated by the spin–rotation mechanism, with a significant additional contribution from the ^{103}Rh CSA at a high magnetic field.

Code availability. The software code for the graphics shown in this paper is available from the authors on reasonable request.

Data availability. The dataset can be accessed at https://doi.org/10.5258/SOTON/D3209 (Harbor-Collins, 2024).

Author contributions. HHC: conceptualisation (equal), data curation (equal), formal analysis (equal), investigation (equal), methodology (equal), software (equal), validation (equal), visualisation (equal), and writing (original draft and review and editing) (equal). MS: conceptualisation (equal), data curation (equal), formal analysis (equal), investigation (equal), methodology (equal), software (equal), visualisation (equal), and writing (original draft and review and editing) (equal). ML: conceptualisation (equal), funding acquisition (equal), investigation (equal), validation (equal), and writing (review and editing) (equal). MHL: conceptualisation (equal), formal analysis (equal), funding acquisition (equal), investigation (equal), project administration (equal), resources (equal), supervision (lead), and writing (original draft and review and editing) (equal).

Competing interests. At least one of the (co-)authors is a member of the editorial board of *Magnetic Resonance*. The peer-review process was guided by an independent editor, and the authors also have no other competing interests to declare.

Disclaimer. Publisher's note: Copernicus Publications remains neutral with regard to jurisdictional claims made in the text, published maps, institutional affiliations, or any other geographical representation in this paper. While Copernicus Publications makes ev-

ery effort to include appropriate place names, the final responsibility lies with the authors.

Financial support. This research has been supported by the European Research Council's H2020 programme (grant no. 786707) and the Engineering and Physical Sciences Research Council (grant nos. EP/P009980/1, EP/P030491/1 and EP/V055593/1).

Review statement. This paper was edited by Patrick Giraudeau and reviewed by two anonymous referees.

References

Aaltonen, T., Ritala, M., and Leskelä, M.: ALD of Rhodium Thin Films from Rh (Acac)$_3$ and Oxygen, Electrochem. Solid St., 8, C99, 2005.

Bajo, S., Alférez, M. G., Alcaide, M. M., López-Serrano, J., and Campos, J.: Metal-Only Lewis Pairs of Rhodium with s, p and d-Block Metals, Chem.-Eur. J., 26, 16833–16845, 2020.

Benn, R., Brenneke, H., and Reinhardt, R.-D.: ^{103}Rh-NMR Bei 9,4 T – Verbesserter Nachweis Infolge Verkürzter Relaxationszeiten Und Selektivem Polarisationstransfer / ^{103}Rh NMR at 9.4 T – Improved Signal Detection Due to Shortened Relaxation Times and Selective Polarisation Transfer, Z. Naturforsch. B, 40, 1763–1765, 1985.

Brevard, C. and Schimpf, R.: Phosphorus-Irradiation INEPT Experiments on Spin-12 Metal Nuclides. Applications to ^{103}Rh, ^{183}W, and ^{57}Fe, J. Magn. Reson., 47, 528–534, 1982.

Brevard, C., Van Stein, G. C., and Van Koten, G.: Silver-109 and Rhodium-103 NMR Spectroscopy with Proton Polarization Transfer, J. Am. Chem. Soc., 103, 6746–6748, 1981.

Buckingham, A. D. and Malm, S. M.: Asymmetry in the Nuclear Magnetic Shielding Tensor, Mol. Phys., 22, 1127–1130, 1971.

Burum, D. P. and Ernst, R. R.: Net Polarization Transfer via a J-ordered State for Signal Enhancement of Low-Sensitivity Nuclei, J. Magn. Reson., 39, 163–168, 1980.

Caló, F. P., Bistoni, G., Auer, A. A., Leutzsch, M., and Fürstner, A.: Triple Resonance Experiments for the Rapid Detection of ^{103}Rh NMR Shifts: A Combined Experimental and Theoretical Study into Dirhodium and Bismuth–Rhodium Paddlewheel Complexes, J. Am. Chem. Soc., 143, 12473–12479, 2021.

Carlton, L.: Chapter 3 - Rhodium-103 NMR, in: Annual Reports on NMR Spectroscopy, vol. 63, edited by: Webb, G. A., Academic Press, https://doi.org/10.1016/S0066-4103(07)63003-8, 49–178, 2008.

Carravetta, M., Edén, M., Zhao, X., Brinkmann, A., and Levitt, M. H.: Symmetry Principles for the Design of Radiofrequency Pulse Sequences in the Nuclear Magnetic Resonance of Rotating Solids, Chem. Phys. Lett., 321, 205–215, 2000.

Chan, A. P., Parkinson, J. A., Rosair, G. M., and Welch, A. J.: Bis(Phosphine)Hydridorhodacarborane Derivatives of 1,1′-Bis(Ortho-Carborane) and Their Catalysis of Alkene Isomerization and the Hydrosilylation of Acetophenone, Inorg. Chem., 59, 2011–2023, 2020.

Chingas, G. C., Garroway, A. N., Bertrand, R. D., and Moniz, W. B.: Zero Quantum NMR in the Rotating Frame: J Cross Polarization in AXN Systems, J. Chem. Phys., 74, 127–156, 1981.

Choi, S.-I., Lee, S. R., Ma, C., Oliy, B., Luo, M., Chi, M., and Xia, Y.: Facile Synthesis of Rhodium Icosahedra with Controlled Sizes up to 12 Nm, ChemNanoMat, 2, 61–66, 2016.

Harbor-Collins, H.: Dataset in support of the paper "H enhanced 103Rh NMR spectroscopy and relaxometry of 103Rhacac in solution", University of Southampton [data set], 2024.

Crocker, C., John Errington, R., S. McDonald, W., J. Odell, K., L. Shaw, B., and J. Goodfellow, R.: Rapid Reversible Fission of a C–H Bond in a Metal Complex: X-Ray Crystal Structure of [RhHCl($Bu^t_2PCH_2CH_2CHCH_2CH_2PBu^t_2$)], J. Chem. Soc. Chem. Commun., 0, 498–499, 1979.

Cummins, H. K., Llewellyn, G., and Jones, J. A.: Tackling Systematic Errors in Quantum Logic Gates with Composite Rotations, Phys. Rev. A, 67, 042308, 2003.

Doddrell, D. M., Pegg, D. T., Brooks, W., and Bendall, M. R.: Enhancement of Silicon-29 or Tin-119 NMR Signals in the Compounds M(CH3)(n)Cl(4−n)M = Silicon or Tin, n = 4, 3, 2) Using Proton Polarization Transfer. Dependence of the Enhancement on the Number of Scalar Coupled Protons, J. Am. Chem. Soc., 103, 727–728, 1981.

Doddrell, D. M., Pegg, D. T., and Bendall, M.: Quasi-Stochastic J Cross-Polarization in Liquids, J. Magn. Reson. (1969), 49, 181–196, 1982.

Dykstra, R. W., Harrison, A. M., and Dombek, B. D.: Multinuclear Nuclear Magnetic Resonance Observations of *H*-cyclopentadienyldicarbonylrhodium (I) Including Heteronuclear Double and Triple Irradiation, Rev. Sci. Instrum., 52, 1690–1696, 1981.

Ernsting, J. M., Gaemers, S., and Elsevier, C. J.: ^{103}Rh NMR Spectroscopy and Its Application to Rhodium Chemistry, Magn. Reson. Chem., 42, 721–736, 2004.

Freeman, R., Frenkiel, T., and Levitt, M. H.: A Simple "Black-Box" Decoupler, J. Magn. Reson. (1969), 50, 345–348, 1982.

Grüninger, K.-D., Schwenk, A., and Mann, B. E.: Direct Observation of 103Rh NMR and Relaxation Investigations by Steady-State Techniques, J. Magn. Reson., 41, 354–357, 1980.

Gullion, T.: The Effect of Amplitude Imbalance on Compensated Carr–Purcell Sequences, J. Magn. Reson., Series A, 101, 320–323, 1993.

Gullion, T., Baker, D. B., and Conradi, M. S.: New, Compensated Carr–Purcell Sequences, J. Magn. Reson. (1969), 89, 479–484, 1990.

Harbor-Collins, H., Sabba, M., Moustafa, G., Legrady, B., Soundararajan, M., Leutzsch, M., and Levitt, M. H.: The ^{103}Rh NMR Spectroscopy and Relaxometry of the Rhodium Formate Paddlewheel Complex, J. Chem. Phys., 159, 104307, https://doi.org/10.1063/5.0165830, 2023.

Harbor-Collins, H., Sabba, M., Bengs, C., Moustafa, G., Leutzsch, M., and Levitt, M. H.: NMR Spectroscopy of a 18O-labeled Rhodium Paddlewheel Complex: Isotope Shifts, ^{103}Rh–^{103}Rh Spin–Spin Coupling, and ^{103}Rh Singlet NMR, J. Chem. Phys., 160, 014305, 2024.

Heaton, B. T., Strona, L., Della Pergola, R., L. Vidal, J., and C. Schoening, R.: Multinuclear Variable-Temperature Nuclear Magnetic Resonance Study of Rhodium Carbonyl Clusters Con-

taining Encapsulated Heteroatoms: Ligand and Metal Polyhedral Rearrangements, J. Chem. Soc. Dalton, 0, 1941–1947, 1983.

Herberhold, M., Daniel, T., Daschner, D., Milius, W., and Wrackmeyer, B.: Mononuclear Half-Sandwich Rhodium Complexes Containing Phenylchalcogenolato Ligands: A Multinuclear (^{1}H, ^{13}C, ^{31}P, ^{77}Se, ^{103}Rh, ^{125}Te) Magnetic Resonance Study, J. Organomet. Chem., 585, 234–240, 1999.

Holmes, S. T., Schoenzart, J., Philips, A., Kimball, J., Termos, S., R Altenhof, A., Xu, Y., A. O'Keefe, C., Autschbach, J., and Schurko, R.: Structure and Bonding in Rhodium Coordination Compounds: A ^{103}Rh Solid-State NMR and Relativistic DFT Study, Chem. Sci., https://doi.org/10.1039/D3SC06026H, 2023.

Hubbard, P. S.: Theory of Nuclear Magnetic Relaxation by Spin-Rotational Interactions in Liquids, Phys. Rev., 131, 1155–1165, 1963.

Levitt, M. H.: Heteronuclear Cross Polarization in Liquid-state Nuclear Magnetic Resonance: Mismatch Compensation and Relaxation Behavior, J. Chem. Phys., 94, 30–38, 1991.

Levitt, M. H., Freeman, R., and Frenkiel, T.: Broadband Heteronuclear Decoupling, J. Magn. Reson. (1969), 47, 328–330, 1982a.

Levitt, M. H., Freeman, R., and Frenkiel, T.: Supercycles for Broadband Heteronuclear Decoupling, J. Magn. Reson. (1969), 50, 157–160, 1982b.

Lutz, M. D. R., Zhong, H., Trapp, N., and Morandi, B.: Synthesis and Reversible H_2 Activation by Coordinatively Unsaturated Rhodium NHC Complexes, Helv. Chim. Acta, 106, e202200199, https://doi.org/10.1002/hlca.202200199, 2023.

Mann, B. E.: The Cinderella Nuclei, in: Annual Reports on NMR Spectroscopy, vol. 23, edited by: Webb, G. A., Academic Press, https://doi.org/10.1016/S0066-4103(08)60277-X, 141–207, 1991.

Maurer, E., Rieker, S., Schollbach, M., Schwenk, A., Egolf, T., and von Philipsborn, W.: Direct Observation of ^{103}Rh-Chemical Shifts in Mono- and Dinuclear Olefin Complexes, Helv. Chim. Acta, 65, 26–45, 1982.

Nielsen, N., Schulte-Herbrüggen, T., and Sørensen, O.: Bounds on Spin Dynamics Tightened by Permutation Symmetry Application to Coherence Transfer in I_2S and I_3S Spin Systems, Mol. Phys., 85, 1205–1216, 1995.

Pegg, D. T., Doddrell, D. M., Brooks, W. M., and Robin Bendall, M.: Proton Polarization Transfer Enhancement for a Nucleus with Arbitrary Spin Quantum Number from n Scalar Coupled Protons for Arbitrary Preparation Times, J. Magn. Reson. (1969), 44, 32–40, 1981.

Pegg, D. T., Doddrell, D. M., and Bendall, M. R.: Proton-Polarization Transfer Enhancement of a Heteronuclear Spin Multiplet with Preservation of Phase Coherency and Relative Component Intensities, J. Chem. Phys., 77, 2745–2752, 1982.

Peng, J. W., Thanabal, V., and Wagner, G.: Improved Accuracy of Heteronuclear Transverse Relaxation Time Measurements in Macromolecules. Elimination of Antiphase Contributions, J. Magn. Reson. (1969), 95, 421–427, 1991.

Rösler, T., Ehmann, K. R., Köhnke, K., Leutzsch, M., Wessel, N., Vorholt, A. J., and Leitner, W.: Reductive Hydroformylation with a Selective and Highly Active Rhodium Amine System, J. Catal., 400, 234–243, 2021.

Sabba, M., Wili, N., Bengs, C., Whipham, J. W., Brown, L. J., and Levitt, M. H.: Symmetry-Based Singlet–Triplet Excitation in Solution Nuclear Magnetic Resonance, J. Chem. Phys., 157, 134302, 2022.

Samultsev, D. O., Semenov, V. A., and Krivdin, L. B.: Four-Component Relativistic Calculations of NMR Shielding Constants of the Transition Metal Complexes. Part 1: Pentaammines of Cobalt, Rhodium, and Iridium, Magn. Reson. Chem., 60, 463–468, 2022.

Schwartz, I., Scheuer, J., Tratzmiller, B., Müller, S., Chen, Q., Dhand, I., Wang, Z.-Y., Müller, C., Naydenov, B., Jelezko, F., and Plenio, M. B.: Robust Optical Polarization of Nuclear Spin Baths Using Hamiltonian Engineering of Nitrogen-Vacancy Center Quantum Dynamics, Sci. Adv., 4, https://doi.org/10.1126/sciadv.aat8978, 2018.

Sheng Loong Tan, N., Nealon, G. L., Moggach, S. A., Lynam, J. M., Ogden, M. I., Massi, M., and Lowe, A. B.: (η^4-Tetrafluorobenzobarrelene)-η^1-((Tri-4-Fluorophenyl)Phosphine))-η^1-(2-Phenylphenyl)Rhodium(I): A Catalyst for the Living Polymerization of Phenylacetylenes, Macromolecules, 54, 6191–6203, 2021.

Widemann, M., Eichele, K., Schubert, H., Sindlinger, C. P., Klenner, S., Pöttgen, R., and Wesemann, L.: Synthesis and Hydrogenation of Heavy Homologues of Rhodium Carbynes: [$(Me_3P)_2(Ph_3P)Rh \equiv E\text{-}Ar^*$] (E = Sn, Pb), Angew. Chem. Int. Ed., 60, 5882–5889, 2021.

Wiedemair, M., Kopacka, H., Wurst, K., Müller, T., Eichele, K., Vanicek, S., Hohloch, S., and Bildstein, B.: Rhodocenium Functionalization Enabled by Half-Sandwich Capping, Zincke Reaction, Diazoniation and Sandmeyer Chemistry, Eur. J. Inorg. Chem., 2021, 3305–3313, 2021.

Wimperis, S.: Broadband, Narrowband, and Passband Composite Pulses for Use in Advanced NMR Experiments, J. Magn. Reson., Series A, 109, 221–231, 1994.

Zhang, Y., Grass, M. E., Habas, S. E., Tao, F., Zhang, T., Yang, P., and Somorjai, G. A.: One-Step Polyol Synthesis and Langmuir–Blodgett Monolayer Formation of Size-tunable Monodisperse Rhodium Nanocrystals with Catalytically Active (111) Surface Structures, J. Phys. Chem. C, 111, 12243–12253, 2007.

Zhukov, I. V., S. Kiryutin, A., V. Yurkovskaya, A., A. Grishin, Y., Vieth, H.-M., and L. Ivanov, K.: Field-Cycling NMR Experiments in an Ultra-Wide Magnetic Field Range: Relaxation and Coherent Polarization Transfer, Phys. Chem. Chem. Phys., 20, 12396–12405, 2018.